Available online at www.sciencedirect.com
SCIENCE DIRECT
Catalysis Today 116 (2006) 169–178
CATALYSIS TODAY
www.elsevier.com/locate/cattod

Influence of the synthesis method on the nanostructure and reactivity of mesoporous Pt/Mn-WO_x-ZrO_2 catalysts

M.L. Hernández [a,b], J.A. Montoya [a,*], P. Del Angel [a], I. Hernández [b], G. Espinosa [a], M.E. Llanos [a]

[a] *Instituto Mexicano del Petróleo, Molecular Engineering Program, Eje Central Lázaro Cárdenas 152, México D.F. 07730, Mexico*
[b] *Universidad Autónoma Metropolitana-Azcapotzalco, Av. San Pablo 180 Col. Reynosa, México D.F. 02200, Mexico*

Available online 27 June 2006

Abstract

The influence of the synthesis method on acid site generation, nanostructure and reactivity of Mn-promoted WO_x-ZrO_2 catalysts was investigated. The materials were synthesized by impregnation (IMP), coprecipitation (COP) and reflux (COP-R and IMP-R), using cetyltrimethylammonium bromide (CTAB) as surfactant in order to promote the textural properties of the catalysts. The Mn-WO_x-ZrO_2 samples were calcined at 800 °C and characterized by X-ray diffraction (XRD), nitrogen adsorption–desorption, laser Raman spectroscopy, ultraviolet–visible (UV–vis) spectroscopy, high-resolution transmission electron microscopy (HRTEM) and energy dispersive spectroscopy (EDS). The Mn-WO_x-ZrO_2 materials were impregnated with 0.3 wt% of platinum (Pt/Mn-WO_x-ZrO_2) in order to enhance H_2 spillover and diminish coke formation and they were evaluated for *n*-hexane hydroisomerization. The XRD results show that the incorporation of 0.5 wt% Mn cation stabilizes the metastable tetragonal zirconia phase and the Rietveld refinement of the crystalline phases shows that only a fraction of tungsten (about 5 wt%) leads to the formation of the WO_3 segregated phase. Laser Raman and UV–vis spectroscopies verify the presence of different tungsten oxide domains, WO_3 crystallites and a WO_x phase not detected by XRD formed by oligomeric and polymeric WO_x clusters. The surfactant assisted methods produce mesoporous materials with narrow pore size distributions, allowing access to the WO_x clusters of suitable domain size for the hydroisomerization reaction. The simultaneous precipitation of tungsten with the formation of hydrous zirconia and manganese generates a larger number of active sites by the formation of polytungstate species on the zirconia surface with sizes and structures suitable for the isomerization of alkenes. Additionally, the coprecipitation-reflux method (COP-R) results in the formation of WO_x species with W=O bonds which generates acid sites suitable and accessible to the *n*-hexane molecule, leading to an increase in the conversion (70%) and selectivity to the high octane biramified products 2,3-dimethyl-butane (2,3-DMB) and 2,2-dimethyl-butane (2,2-DMB). It was found that besides the role of Mn in the stabilization of the tetragonal phase, this cation promotes the catalytic activity of these materials.

Keywords: Tungstated zirconia; Mn; WO_x nanostructures; Coprecipitation; Impregnation; *n*-Hexane hydroisomerization; HRTEM–EDS

1. Introduction

Isomerization catalysts are normally bifunctional solids which consist of a solid acid such as zeolites, sulfated zirconia, tungstated zirconia, etc., as well as a metallic function, normally platinum. Among these systems, WO_x/ZrO_2 solids have attracted attention because they exhibit higher activity than zeolitic catalysts at moderate reaction temperatures [1,2], which is a desirable condition because branched isomers are thermodynamically favored at low reaction temperatures. The incorporation of tungsten into the zirconia enhances the acid strength of these solids by means of the formation of WO_x nanostructures, which stabilize the protons responsible for the Brönsted acidity [3,4].

Since the preparation of tungstated zirconia by impregnation of hydrated zirconia was reported by Hino and Arata [5], several investigations about the influence of the preparative method on the activity of WO_x/ZrO_2 materials have been reported [1,2,6]. Some of the general conclusions are that the incorporation of tungsten into the zirconia favors the formation of the tetragonal phase, inhibits sintering of the support and enhances the acid strength of these solids by the slight reduction of the WO_x species. These works have found that the catalytic properties of the tungstated zirconia are strongly influenced by

* Corresponding author.
E-mail address: amontoya@imp.mx (J.A. Montoya).

0920-5861/$ – see front matter © 2006 Published by Elsevier B.V.
doi:10.1016/j.cattod.2006.02.084

the preparative method, in part because it determines the size and local structure of the tungstates formed on the surface.

Besides its acidic properties, previous studies have pointed out that the mesoporous structure of tungstated zirconia favors the dispersion of the tungsten species, improves the transport of reactants and products on the solid and avoids secondary reactions promoted by diffusion constraints that slow down the removal of initial isomerization products from the catalyst [7–9]. We have previously shown that the mesoporous structure could be suitably modified by the addition of a surfactant [9]. In addition, it has been found that the incorporation of promoters such as Pt, Pd, Fe, Al, Ga or Mn, to the tungstated zirconia, generates a more effective function of the solid [9–15]. Some other authors have remarked on the importance of the study of additives on the catalytic performance of the WO_x/ZrO_2 materials, or their synergistic actions [14]. Thus, this work was focused on the role of Mn as promoter on WO_x/ZrO_2 materials with mesoporous structures obtained by means of surfactant assisted synthesis.

Moreover, from the viewpoint of acid catalysis, the characterization of the WO_x nanostructures formed on the zirconia surface is of importance since this segregated tungstated phase is believed to be responsible for the formation of catalytic active sites involving in the isomerization reactions.

In this work, several methods of synthesis were compared in order to investigate the influence of the synthesis procedure and manganese incorporation on the textural properties and nanostructure of mesoporous Pt/Mn-WO_x-ZrO_2 solids, as well as its application as acidic catalysts in the *n*-hexane hydroisomerization reaction.

2. Experimental

2.1. Catalyst preparation

A series of mesoporous Mn-WO_x-ZrO_2 oxides were prepared by methods similar to those described by Santiesteban et al. [2] using the chemicals (Aldrich): zirconyl nitrate $ZrO(NO_3)_2{\cdot}xH_2O$, manganese nitrate $Mn(NO_3)_2{\cdot}xH_2O$ and ammonium metatungstate $(NH_4)_6W_{12}O_{39}{\cdot}xH_2O$. A surfactant was employed as an aqueous solution of cetyl-trimethylammonium bromide (CTAB) at 20 wt% with a fixed CTAB/ZrO_2 = 3.0 molar ratio. The nominal composition for all the oxides was 0.5 wt% Mn/20 wt% W/ZrO_2.

2.1.1. Mn-WO_x-ZrO_2 oxides prepared by impregnation

An aqueous solution of zirconyl nitrate (0.2 M) was mixed with CTAB (20 wt% in water) and manganese nitrate in solution (0.5 M) at 80 °C. The amounts of chemicals were calculated so as to obtain 1 g of the metallic mixed oxide. The precipitation was achieved by adding dropwise about 3 ml of NH_4OH (10 M) at 40 °C until a pH 11 value was reached. The precipitate was washed several times with about 50 ml of distilled water each time until excess surfactant was eliminated; this washing procedure was employed in all samples. Then, the precipitate was filtered and dried at 110 °C for 24 h. The elimination of the excess surfactant was monitored by a rapid XRD screening (Bruker-Axs D8 Discover) of the dried samples. The hydrous zirconia was impregnated with an ammonium metatungstate solution (0.005 M) in adequate concentration to obtain a 20 wt% tungsten loading and the solid was dried at 110 °C for 16 h. The calcination treatment was performed in static air at 800 °C for 4 h. This sample was labeled as ZWMn-IMP.

2.1.2. Mn-WO_x-ZrO_2 oxides prepared by coprecipitation

Aqueous solutions of CTAB (20 wt%), zirconyl nitrate (0.2 M) and manganese nitrate (0.5 M) were mixed in adequate concentrations with the tungsten solution (0.025 M) at 80 °C. Then, about 3 ml of NH_4OH (10 M) was added dropwise until pH 11 to precipitate the hydrous zirconia. The precipitate was washed repeatedly as described above and then filtered and dried at 110 °C for 24 h. The calcination treatment was performed in static air at 800 °C for 4 h. This catalyst was labeled as ZWMn-COP.

2.1.3. Mn-WO_x-ZrO_2 oxides prepared by reflux

These catalysts were prepared by impregnation or coprecipitation according to the conditions and procedures described above, but the difference was that the chemical mixtures were refluxed before the precipitation of the hydrous zirconia.

The catalyst prepared by impregnation-reflux was obtained by refluxing the mixture of aqueous solutions of zirconyl nitrate, CTAB and manganese nitrate at 90 °C for 16 h. After the precipitation with NH_4OH at pH 11 and 40 °C, the materials were washed, filtered and dried at 110 °C for 24 h. The dried solid was impregnated with an ammonium metatungstate solution (0.005 M) to obtain a 20 wt% tungsten loading and dried at 110 °C for 16 h.

The catalyst prepared by coprecipitation-reflux was obtained by refluxing aqueous solutions of zirconyl nitrate, CTAB and manganese nitrate with the solution of ammonium metatungstate solution (0.025 M) at 90 °C for 16 h. After the coprecipitation with NH_4OH at pH 11, the materials were washed, filtered and dried at 110 °C for 24 h.

The resulting materials were also calcined at 800 °C in static air and they were denoted as ZWMn-IMP-R and ZWMn-COP-R, respectively.

2.2. Catalyst characterization

Mn-WO_x-ZrO_2 nanostructured mixed oxides were characterized by X-ray powder diffraction (XRD), HRTEM, EDS, nitrogen adsorption–desorption, UV–vis spectroscopy and Raman spectroscopy. The X-ray diffraction patterns were obtained using a Bruker-Axs D8 Discover with General Area Detector Diffraction Systems (GADDS, two-dimensional detector) diffractometer fitted with a Cu tube (40 kV, 40 mA), X-ray beam size of 500 μm, using the combinatorial approach for both measurements and patterns evaluation. For the Rietveld analysis the diffraction patterns were measured using a Siemens D-500 diffractometer calibrated for high resolution with a NIST 1976 (α-Al_2O_3) flat-plate intensity standard and LaB_6 (NIST standard reference material 660a)

with angular accuracy between ±0.013 Å, using a step size = 0.02°, a step time = 10 s and Cu $K\alpha_{1,2}$ radiation. The refinement of the crystalline phases was done by using the FULLPROF-3.5d program. The X-ray fluorescence quantitative analysis for the elemental composition of samples was carried out using a SRS3000 Siemes spectrometer.

The oxides were also studied by high-resolution transmission electron microscopy (HRTEM). The micrographs and EDS were obtained in a TECNAI F30 Super-Twin with Schottky type field emission gun operating at 300 kV. In order to prepare the materials for observation, the powder samples were ultrasonically dispersed in ethanol and supported on holey carbon coated copper grids. HRTEM digital images were obtained using digital micrograph software from GATAN. The lattice distances were compared with JCPDS files of the tetragonal zirconia (79-1769) and monoclinic tungsten oxide (83-0951).

The nitrogen adsorption isotherms and BET surface areas were measured at 77 K with a Micromeritics ASAP 2405 equipment with a deviation of ±6 m^2/g. Prior to the measurements the samples were out-gassed at 350 °C for 15 h under vacuum. The pore size distribution was calculated following the method developed by Barrett, Joyner and Halenda (BJH method) using the desorption branch of the isotherm.

Ultraviolet–visible (UV–vis) diffuse reflectance spectra were obtained using a Varian (Cary 1G) spectrophotometer for the data handling with a diffuse reflectance integration sphere accessory. Raman spectra of the Mn-WO_x-ZrO_2 catalysts were recorded in the 100–1200 cm^{-1} wave number range using a ThermoNicolet Raman apparatus (Almega model) equipped with a Nd:YVO4DPSS laser source. The excitation line of the laser was 532 nm and the laser power was of 25 mW.

2.3. Catalytic activity

Catalytic activity was measured for the *n*-hexane hydroisomerization reaction over the Pt/Mn-WO_x-ZrO_2 catalysts calcined at 800 °C. This evaluation was performed using a Combinatorial Multi Channel Fixed Bed Reactor (MCFBR) (Symyx). This equipment is appropriate to evaluate the activity and selectivity of 48 samples in parallel by applying high-throughput testing techniques with a matrix arrangement of 6 × 8. Briefly, this system consists of six reactor heads each one containing a set of eight microreactors of approximately 4 mm of inner diameter and 47 mm length. The six reactor heads are connected independently to six chromatographs (Agilent, 6850 Series) each equipped with an SPB-1 capillary column (Supelco) with a length of 100 m, a diameter of 0.32 mm and a film thickness of 0.25 μm and a flame ionization detector (FID) for the analysis of products. Catalysts samples of 100 mg diluted in 200 mg of inert silicon carbide were loaded in each well and fixed into the reactor heads. Pretreatment of the catalysts was carried out in situ prior to the activity test and it consisted of a drying–reduction program, drying the samples at 260 °C for 2 h in helium (200 cm^3/min) followed by reduction in a hydrogen flow (200 cm^3/min) at 350 °C for 2 h. Hydrogen and *n*-hexane flows were adjusted to give a $H_2/n\text{-}C_6$ = 1.47 molar ratio. The experimental conditions for the hydroisomerization of *n*-hexane were as follows: reaction pressure of 0.689 MPa, reaction temperature of 220 and 260 °C, the total feed composition was a mixture of H_2 = 0.269 mol/h, He = 0.135 mol/h and a liquid flow of *n*-hexane = 0.184 mol/h, giving a WHSV = 3.695 for every single well. The $H_2/n\text{-}C_6$ molar ratio was 1.469, which is very close to that used in the industrial process.

The catalytic evaluation procedure is fully automated, and for every run the pressure, reactor and accessory temperature and reactant flows are set and controlled in real time. When the experimental conditions are reached, the first set of six reaction products are analyzed simultaneously in the six GC's. The analysis time is 10.7 min, and ones completed the next injection proceeds, and on the process is repeated until the eight sets are analyzed. The 48 chromatograms are saved in a database. In this way every row of six catalysts are evaluated simultaneously and at the same reaction time, however the next set has seen 10.7 additional minutes of reaction time. Therefore, the total time for one experiment run is about 90 min. To determine if the deactivation is important the catalysts are evaluated in different well positions. In this particular type of catalyst it was found that deactivation by carbon deposition was not important at least during the run experiment.

The surface concentration of tungsten was calculated from the measured surface area, as follows: W concentration (W atom/nm^2) = [WO_3 loading (wt%)/100]/231.8 (formula weight of WO_3) × 6.023 × 10^{23}/[BET surface area (m^2/g) × 10^{18}] as it was reported in ref. [16].

3. Results

3.1. Textural properties

The nitrogen isotherms at 77 K for the Mn-WO_x-ZrO_2 catalysts prepared by different methods and calcined at 800 °C are shown in Fig. 1A. All of the isotherms were of type IV (IUPAC classification) with a hysteresis loop characteristic of mesoporous solids with an open pores system. However, the porosity of the samples prepared by tungsten impregnation is different from the materials synthesized by coprecipitation, since the impregnation material presents a different shape of the hysteresis loop compared to the hysteresis obtained for the coprecipitated samples, which shows a flat part (p/p_o from 0.7 to 0.9) characteristic of materials with narrow pore size distributions (PSD). Fig. 1B shows the pore size distributions and it is observed that the surfactant assisted synthesis leads to the formation of solids with narrow and monomodal pore size distributions, but the sharpest and narrowest PSD is obtained for the sample ZWMn-COP-R.

Table 1 summarizes the texture properties, Mn and tungsten concentration (determined by X-ray fluorescence quantitative technique) for the Mn-WO_x-ZrO_2 catalysts calcined at 800 °C. The total tungsten concentration as WO_3 was used for calculating the tungsten surface density. It was observed that

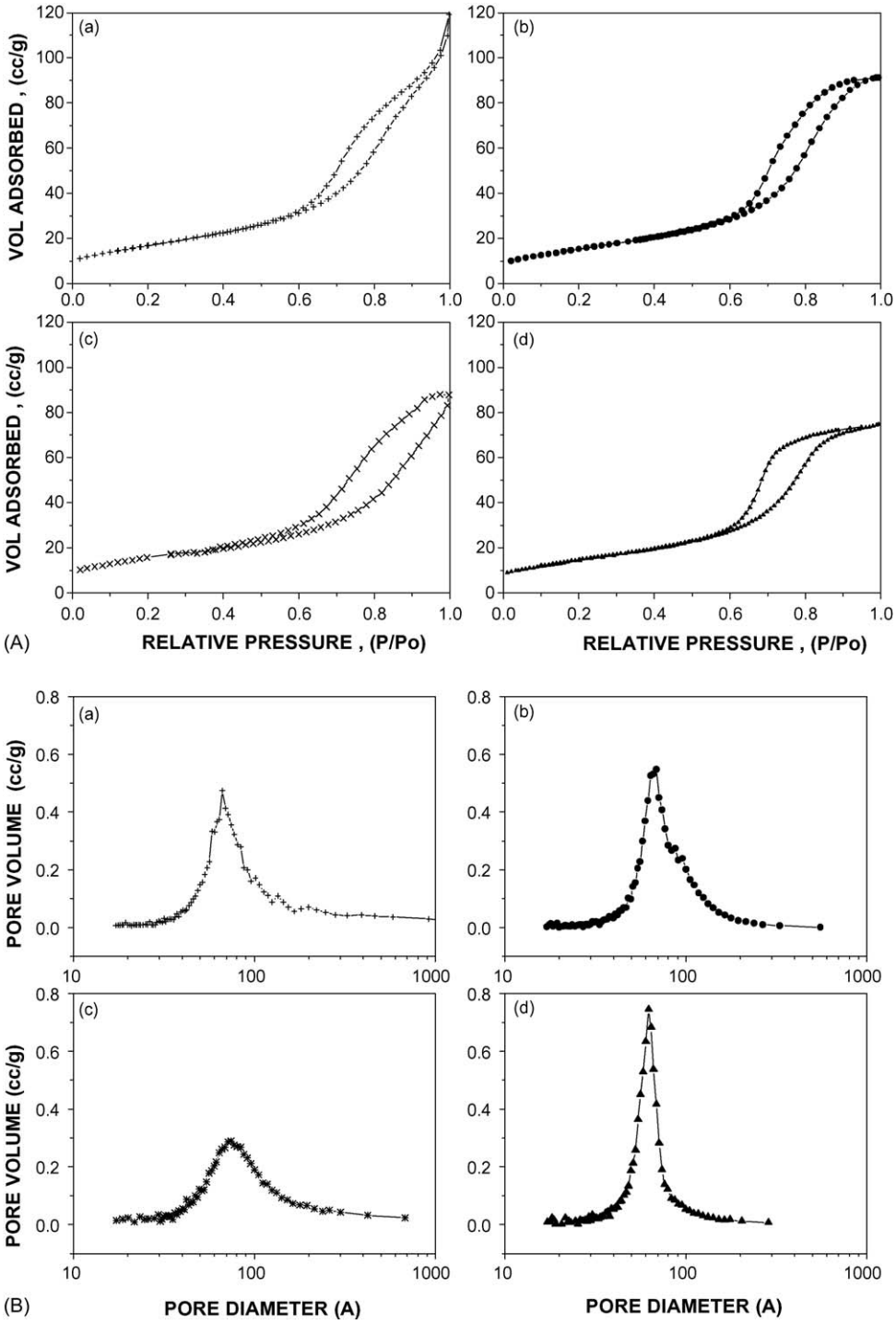

Fig. 1. (A) Adsorption–desorption isotherms and (B) PSD of N_2 at 77 K of Mn-WO_x-ZrO_2 samples prepared by different methods: (a) ZWMn-IMP, (b) ZWMn-COP, (c) ZWMn-IMP-R and (d) ZWMn-COP-R.

these synthesis procedures lead to mesoporous solids with specific surface areas in the range of 44–55 m^2/g (± 6 m^2/g), pore diameters between 60 and 89 Å and pore volume between 0.12 and 0.19 cm^3/g. The specific surface area is similar for the catalysts, but the impregnation method generates higher pore size materials. These results suggest that the method of tungsten incorporation, surfactant and refluxing procedure drastically affects the texture properties of the Mn-WO_x-ZrO_2 catalysts.

The Mn-WO_x-ZrO_2 catalysts exhibited a range of WO_x surface densities from about 9 to 12 W/nm^2 that correspond to higher densities than from the formation of a theoretical two-dimensional polytungstate monolayer, which produces the growth of the domains up to the segregation of crystalline WO_3. It was observed that the materials synthesized by the coprecipitation method provide higher WO_x surface densities than those prepared by impregnation.

Table 1
Manganese and tungsten concentrations, tungsten surface density (δ_W), surface area and porosity of Mn-WO_x-ZrO_2 samples calcined at 800 °C

Catalyst	Mn[a] (wt%)	W[a] (wt%)	δ_W[b] (W atoms/nm^2)	S_g BET (m^2/g)	V_p[c] (cm^3/g)	D_p[c] (Å)
ZW-COP	0	15.89	9.5	55	0.14	66
ZWMn-IMP	0.43	15.94	10.0	52	0.19	89
ZWMn-IMP-R	0.46	16.95	11.3	49	0.15	78
ZWMn-COP	0.45	15.36	10.7	47	0.14	71
ZWMn-COP-R	0.48	16.30	12.1	44	0.12	60

[a] Estimated from X-ray fluorescence.
[b] Estimated from WO_3 content and BET surface area.
[c] BJH desorption.

3.2. Structure

3.2.1. X-ray diffraction and Rietveld refinement

Fig. 2 shows the XRD patterns of the Mn-WO_x-ZrO_2 samples calcined at 800 °C, measured with a D8 Discover diffractometer for combinatorial approach, these patterns are directly comparable since they were measured with the same experimental conditions. The diffraction patterns show the tetragonal-ZrO_2 phase and the formation of monoclinic-WO_3 in all samples. For the sample without Mn (ZW-COP), the formation of monoclinic-ZrO_2 is observed, indicating that the incorporation of 0.5 wt% Mn into WO_x-ZrO_2 samples promotes the stability of zirconia in the tetragonal crystalline phase, and hinders the crystallographic transformation from the metaestable tetragonal phase to the monoclinic phase, even at 800 °C.

The Rietveld analysis was applied to the diffraction patterns measured under special conditions, as it was described previously. The quantitative phase analysis was done for the tetragonal zirconia, monoclinic zirconia and monoclinic tungsten oxide in order to obtain the phase concentration in wt% and the average crystallite sizes, as well as to measure the reticular parameters for each crystallographic phase. The complete results for samples synthesized by coprecipitation are summarized in Table 2. It was found that only a fraction (3–7 wt% as WO_3) of the tungsten loaded (20 wt% as WO_3) on each sample forms crystalline bulk-WO_3, indicating that the major part of WO_x is dispersed forming clusters with a diffraction domain size below 3 nm which are not detectable by XRD. The crystallite size of the tetragonal-ZrO_2 phase formed in the samples was stabilized with an average diameter of 18 nm and was independent of the synthesis method or the W or Mn cations incorporation. With regard to the tetragonal-ZrO_2 cell parameters measured by Rietveld analysis it was found that W or Mn incorporation did not modify the cell parameters with respect to the ZrO_2 standard, which suggests that that tungsten did not enter into the zirconia lattice. However, it is important to note that the XRD technique is a bulk characterization, and it is not able to detect the cation incorporation into the surface cells. So it is possible that a fraction of W and Mn remains in the surface tetragonal-ZrO_2 cells.

The refinement of a blank sample without W is also included, labeled as ZrO_2-Mn (the diffraction pattern is not shown in Fig. 2), and was prepared with the purpose of studying the effect of the manganese on the ZrO_2. It was observed that the Mn (0.5 wt%) is able to avoid the tetragonal–monoclinc transformation keeping the nanocrystal size of about 18 nm.

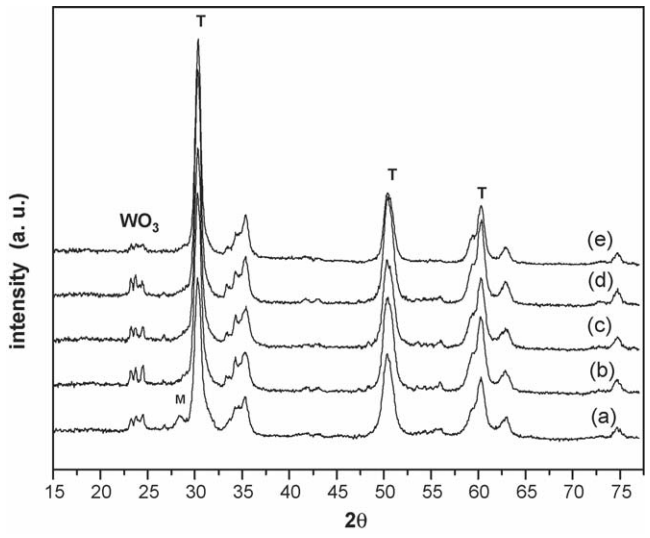

Fig. 2. XRD patterns of catalysts calcined at 800 °C synthesized from different methods (T, M: tetragonal or monoclinic zirconia and WO_3: monoclinic): (a) ZW-COP, (b) ZWMn-IMP, (c) ZWMn-IMP-R, (d) ZWMn-COP and (e) ZWMn-COP-R.

3.2.2. Raman spectroscopy

Raman measurements were carried out in order to investigate the nature of the WO_x surface nanostructures formed on the Mn-ZrO_2 materials, which cannot be detected by XRD. The Raman spectra for Mn-WO_x-ZrO_2 oxides synthesized by impregnation and coprecipitation in the range of 100–1200 cm^{-1}, including the refluxing coprecipitated sample (ZWMn-COP-R) are given in Fig. 3. The spectra show the typical bands at 270, 714 and 806 cm^{-1}, which has been attributed to the formation of the crystalline WO_3 phase and corresponds to W–O–W deformation, W–O bending and W–O stretching modes, respectively [4,6,13]. Additionally it was observed that the samples synthesized by coprecipitation (ZWMn-COP and ZWMn-COP-R) exhibit a higher intensity of the broad band at about 990 cm^{-1}, associated to the symmetric stretching mode of terminal W=O bonds which are present in monotungstate and polytungstate species [6,13]. Iglesia and coworkers have suggested that well-dispersed WO_x structures form two-dimensional oligomers that are responsible for the formation of active sites for the isomerization reactions [4]. It has been also found that polytungstate clusters are formed even at low W concentrations. At higher tungsten loadings the

Table 2
Rietveld refinement results for samples synthesized by coprecipitation: ZrO_2-Mn, ZW-COP and ZWMn-COP

Sample	Crystalline phase	Lattice parameters (Å)			Phase composition (wt%)	Crystallite size (nm)
		a	*b*	*c*		
ZrO_2-Mn	ZrO_2-tetragonal	3.59	3.59	5.16	100	18
	ZrO_2-monoclinic	–	–	–	0	–
	WO_3-monoclinic	–	–	–	0	–
ZW-COP	ZrO_2-tetragonal	3.59	3.59	5.17	91.2	15
	ZrO_2-monoclinic	5.14	5.13	5.37	5.6	19
	WO_3-monoclinic	7.32	7.52	7.71	7.2	72
ZWMn-COP	ZrO_2-tetragonal	3.59	3.59	5.18	97.1	21
	ZrO_2-monoclinic	–	–	–	0	–
	WO_3-monoclinic	7.29	7.52	7.68	2.9	36

formation of interconnected polytungstate clusters is increased as is the density of catalytically active sites on the surface, before the formation of the inactive WO_3 phase [14].

The formation of tetragonal zirconia was identified only by the weak shoulders at about 450 and 647 cm^{-1} [13], since some of the bands corresponding to the tetragonal zirconia are in the same position than that ones corresponding to the WO_3. The characteristics bands for the monoclinic-ZrO_2 phase were not observed. Finally, the presence of $MnWO_4$ was identified by the band at 886 cm^{-1} [17] only in the samples prepared by coprecipitation. It has been suggested that this compound hinders the dispersion of promoters [17]; however our results indicate that this component does not modify the promoting effect of manganese.

3.2.3. UV–vis spectroscopy

UV–vis diffuse reflectance absorption spectra, recorded in air, of Mn-WO_x-ZrO_2 samples prepared by impregnation and coprecipitation, as well as the WO_3 and ZrO_2 standards with a large crystallite size, are given in Fig. 4. It can be seen that the WO_3 standard spectra shows the optical adsorption edge energy at 2.59 eV. The adsorption edge energy values were determined for all the samples using the method reported by Barton et al. [4]. The adsorption edge energy at 2.59 eV corresponds to the transition of electrons from the O 2p valence band to the W^{6+} 5d conduction band of the monoclinic-WO_3 crystallographic phase. For ZrO_2 the adsorption edge energy was calculated at 5.4 eV in agreement with the literature data [4], showing that ZrO_2 is almost an insulating material. An absorption tail is observed due to the phonons contribution of the ZrO_2 crystal lattice. The adsorption edge comes from the transitions from O^{-2} to Zr^{4+} charge transfer, due to the excitation of electrons from the valence band (having O 2p character) to the conduction band (having Zr 4d character). With regard to the UV–vis spectra of both ZWMn-IMP and ZWMn-COP samples, the adsorption edge contribution of the monoclinic-WO_3 bulk, which was identified and quantified by XRD, and the adsorption edge of the WO_x polytungstate clusters dispersed over the tetragonal-ZrO_2 nanocrystals are clearly seen. It is also observed that the intensity of the WO_x adsorption edge is higher for the ZWMn-IMP sample than the intensity of the ZWMn-COP sample indicating that the domaine size of the polytungstate clusters is larger for the ZWMn-IMP sample prepared by impregnation. The adsorption edge energy of the ZWMn-IMP and the ZWMn-COP samples were calculated at 3.2 and 3.6 eV, respectively, and correspond to the ligand-to-metal charge

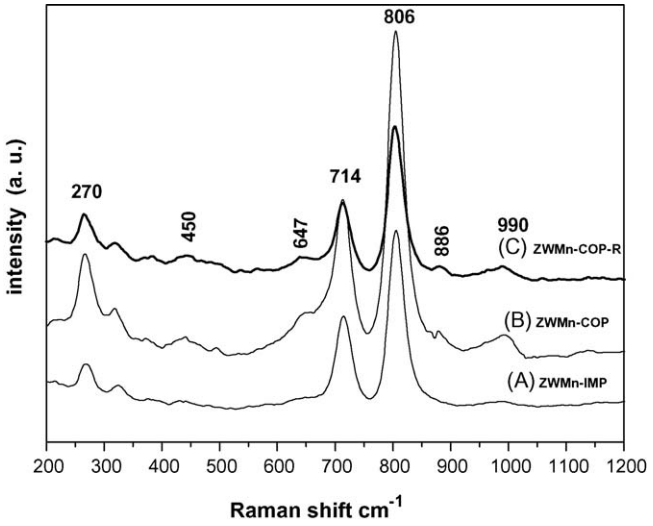

Fig. 3. Raman spectra in the 200–1200 cm^{-1} range of samples: (A) ZWMn-IMP, (B) ZWMn-COP and (C) ZWMn-COP-R.

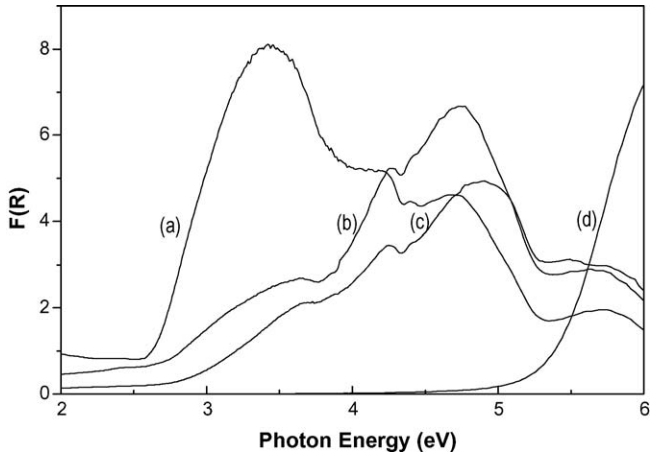

Fig. 4. Diffuse reflectance UV–vis absorption spectra of: (a) WO_3-std, (b) ZWMn-IMP, (c) ZWMn-COP and (d) ZrO_2.

transfer ($O_{2p} \rightarrow W_{5d}$–$O_{2p}$). The energy necessary for this transition depends strongly on WO_x concentration and oxidation temperature [4].

3.2.4. High-resolution transmission electron microscopy and EDS

In order to study the morphology, nanostructure and chemical composition of the Mn-WO_x-ZrO_2 aggregates, the ZWMn-COP sample was analyzed by HRTEM and EDS in the TECNAI F30 electron microscope. The electron microscopy techniques allows the direct observation of the crystallite shape and size, phase identifications, atomic planes irregularities, chemical composition and the grain boundary involved in the generation of porosity. This information is complementary to that obtained by XRD, N_2 adsorption and Raman spectroscopy for reaching a deep characterization of the catalysts.

Fig. 5 shows a typical irregular morphology of these materials, which show a crystallite size distribution from 8 to about 30 nm, in concordance with the average crystallite size for the tetragonal zirconia obtained by the Rietveld refinement (Table 2). It is also seen that the porosity arises from intrananocrystals spaces, the particles being in contact form a three-dimensional structure with disordered porosity.

Fig. 6 and other high-resolution images, which are not shown, show the presence of tetragonal-ZrO_2, monoclinic-WO_3 and WO_x clusters, and some crystallites corresponding to the monoclinic-ZrO_2 phase. The most abundant phase corresponds to the tetragonal zirconia crystallographic phase. The monoclinic-WO_3 crystals are in a wide size distribution dispersed over the tetragonal-ZrO_2 nanocrystals, as well as in very small clusters which could correspond to the WO_x species not observed by XRD. These species are in the sizes range between 4 and 8 Å and they are observed with different contrast as black dots in Fig. 6. These types of clusters were analyzed carefully by serial focus with the HRTEM technique in order to verify their presence [18].

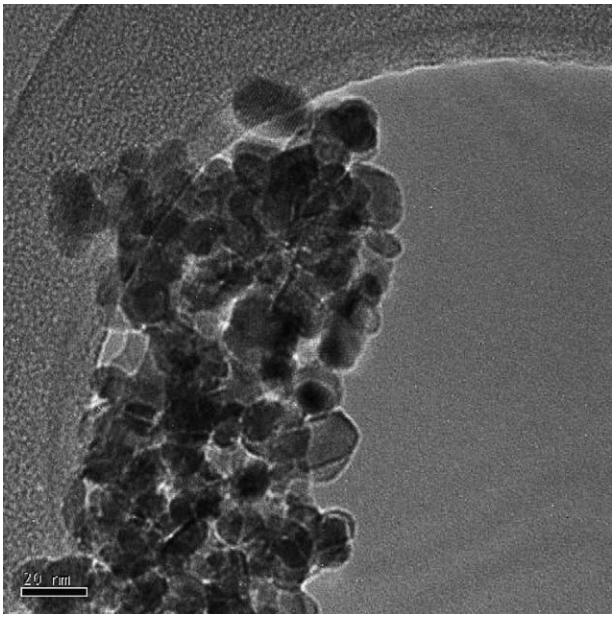

Fig. 5. Typical TEM image at low magnification of the nanostructured mixed oxides Mn-WO_x-ZrO_2 showing the morphology of sample ZWMn-COP.

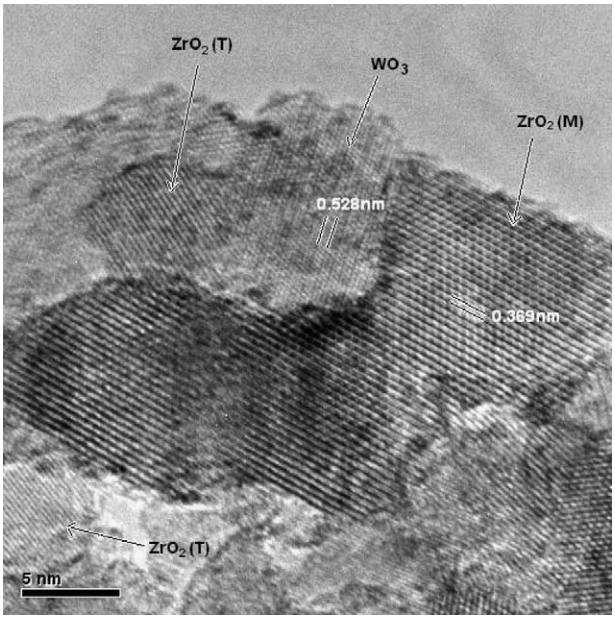

Fig. 6. Typical HRTEM image of sample ZWMn-COP composed by irregular and defective crystallites of tetragonal-ZrO_2 (T), monoclinic-ZrO_2 (M) and monoclinic-WO_3.

EDS semiquantitative analyses were obtained at different regions in the high-resolution mode and these results confirm the presence of the Mn, W, Zr and O at the regions analyzed. The concentration results of these elements in every analysis were close to the elemental bulk concentration determined by FXRD (Table 1). A typical EDS spectrum is shown in Fig. 7, where the energy emission lines are assigned to the elements present in the sample.

3.3. Catalytic activity

The catalytic properties of the Pt/Mn-WO_x-ZrO_2 samples prepared by different methods were evaluated for the *n*-hexane hydroisomerization reaction. The *n*-hexane conversions obtained

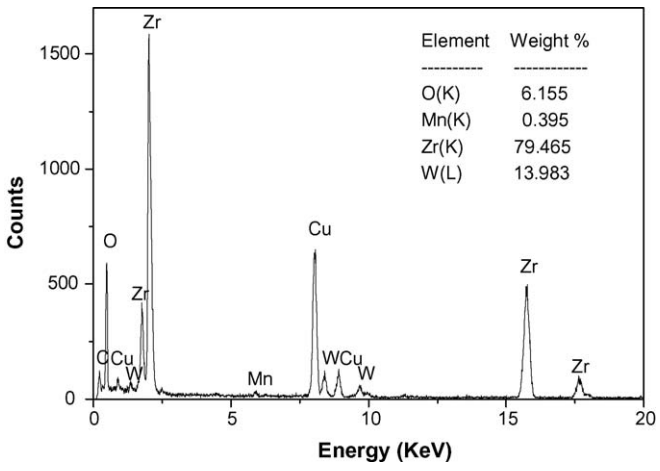

Fig. 7. Chemical composition (EDS) obtained from the region showed in Fig. 6.

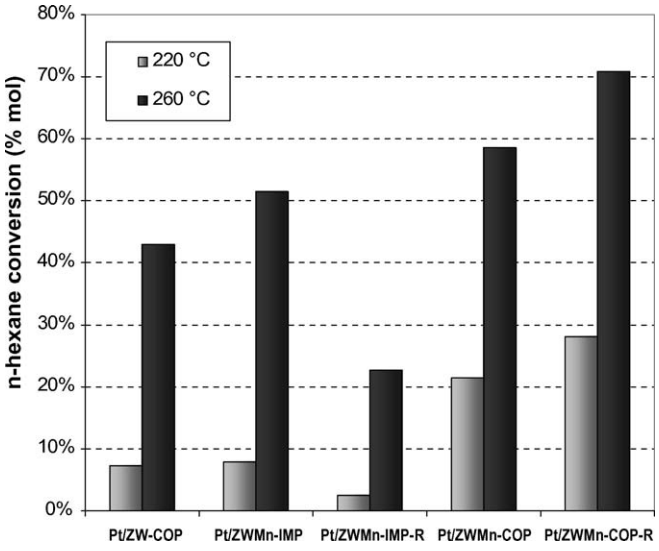

Fig. 8. *n*-Hexane conversion in the hydroisomerization reaction at 0.689 MPa, 220 and 260 °C over Pt/Mn-WO_x-ZrO_2 catalysts prepared by different methods.

at 220 and 260 °C are shown in Fig. 8. The *n*-C_6 isomerization data were interpreted kinetically in terms of a reversible first-order reaction, using the rate expression:

$$k_A = \left(\frac{1}{t}\right)(X_e)\left[-\ln\left(1-\frac{X}{X_e}\right)\right]$$

where X_e is the equilibrium conversion, $1/t$ the superficial contact time in molecules of *n*-C_6 feed/cm^2 of catalyst s and k_A is the forward rate constant in molecules of *n*-C_6 isomerized/cm^2 of catalyst s. In order to compare the catalytic data using reaction rates, forward isomerizaton rates based on mass (k_w) were calculated as reported by Santiesteban et al. [2]. The results are reported in Table 3, where $k_w = (WHSV)(X_e) \times [-\ln(1 - X/X_e)]$. The equilibrium conversion (X_e) at 260 °C was 85.9 mol%. Comparison of the isomerization rates, k_w; among the catalysts indicates that the coprecipitated catalysts show higher density of active sites than the catalysts prepared by impregnation.

The selectivity toward the different isomers is shown in Fig. 9. It is observed that the catalytic conversion of the Pt/Mn-WO_x-ZrO_2 materials is very sensitive to the synthesis method. The samples prepared by coprecipitation yield higher *n*-hexane conversion in the range of 50–70%, than those prepared by impregnation, with conversions from 27 to 56%. It should be noticed that the ZWMN-COP-R catalyst shows higher conversion even at 220 °C than the ZWMn-IMP-R sample does at 260 °C. The results reveal that the higher contact of

Table 3
n-Hexane isomerzation rates based on mass (k_w) over WO_x-ZrO_2 catalysts at 260 °C

Catalyst	k_w[a] (g *n*-C_6/g catalyst h)
ZW-COP	2.79
ZWMn-IMP	3.38
ZWMn-IMP-R	1.20
ZWMn-COP	4.71
ZWMn-COP-R	7.06

[a] $k_w = (WHSV)(X_e) \times [-\ln(1 - X/X_e)]$.

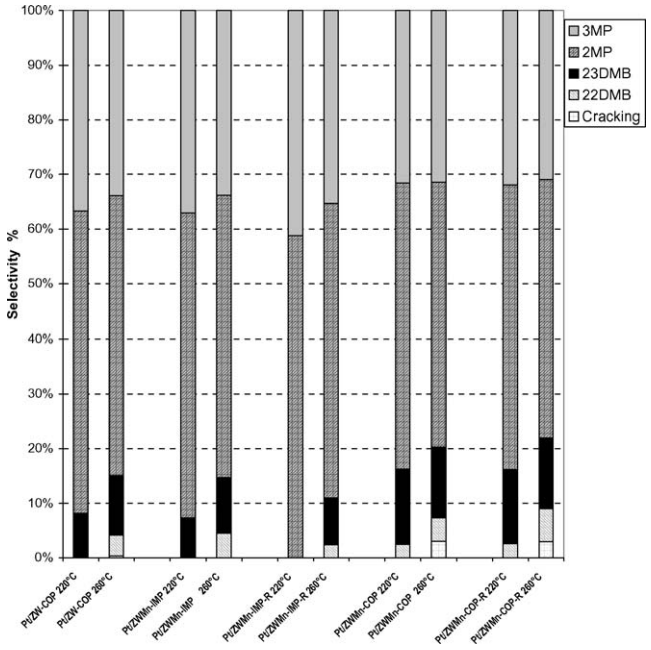

Fig. 9. Isomers distribution in *n*-hexane hydroisomerization reaction at 220 and 260 °C.

tungsten with the zirconia precursors before the precipitation, by means of the refluxing procedure, generates a higher density of acid active sites. The catalyst prepared by coprecipitation and reflux (ZWMn-COP-R) showed the highest activity (conversion = 70%), but the refluxed sample prepared by impregnation, ZWMn-IMP-R, showed lowest activity. It is worthwhile to note that the sample prepared by coprecipitation and prepared with manganese (ZWMn-COP) show higher activity than the sample prepared without manganese (ZW-COP), suggesting a possible role as a promoter of this cation in *n*-hexane isomerization reactions.

With regard to the selectivity, and in agreement with the most accepted mechanism [10,20] for the *n*-C_6 isomerization, 2-methyl-pentane (2MP) and 3-methyl-pentane (3MP) are the primary isomers easily formed (at low conversions). After that, 2,3-dimethyl-butane (2,3-DMB) appears (at higher conversions), and 2,2-dimethyl-butane (2,2-DMB), is considered as a secondary product. It was observed that all of the catalysts evaluated at 260 °C show the formation of the four *n*-hexane isomers 2MP and 3MP followed by 2,3-DMB and 2,2-DMB, but the catalysts synthesized by the coprecipitation technique increases the formation of high octane 2,3-DMB and 2,2-DMB isomer, even at 220 °C.

4. Discussion

The influence of the synthesis method and Mn incorporation on the catalytic behavior of Pt/Mn-WO_x-ZrO_2 materials was studied. Additionally, the effect of the addition of manganese over the structural stability and catalytic behavior in the *n*-hexane hydroisomerization reaction was also evaluated.

It was found that the simultaneous coprecipitation of tungsten with the hydrous zirconia and refluxing the chemical precursors allows a suitable interaction between the hydrous

zirconia, manganese and tungsten. The incorporation of a surfactant (CTAB) prevents the aggregation and growth of particles, modifying the nanostructure of the Mn-tungstated zirconia hydroxides. Crystal growth, phase transformation and sintering processes are controlled during the thermal oxidation treatment of zirconia hydroxide and after calcination at 800 °C the Mn-WO_x-ZrO_2 materials exhibit a monomodal and narrow pore size distribution with specific surface areas between 44 and 55 m^2/g. Although the surfactant/ZrO_2 molar ratio was constant for all the materials, the PSD and pore diameter were different, indicating that the synthesis method affects the textural properties of the Mn-WO_x-ZrO_2. The morphology and nanostructure the Mn-WO_x-ZrO_2 aggregates was analyzed by HRTEM, and it was found (Fig. 5) that they has an irregular morphology and it is also possible to observe that the porosity arises from the intrananocrystals spaces since the particles are in contact forming a three-dimensional structure. These irregular aggregates of tetragonal-ZrO_2 present a highly defective surface which is suitable to anchor strongly the WO_x clusters, preventing the monoclinc-WO_3 growth. In addition, this morphology enhances the accessibility of the WO_x species to the hydrocarbon reactants.

The study of the tungsten phases formed on the zirconia surface was performed by XRD and spectroscopic techniques. The results show that the interaction between the hydrous zirconia with manganese, tungsten and surfactant seems to prevent the particles growth retarding the transformation to the monoclinic phase. It seems that the incorporation of manganese (0.5 wt%) improves the stabilization of the tungstated zirconia at temperatures as high as 800 °C (Fig. 2), although, traces of monoclinic zirconia were found by HRTEM. The characterization by X-ray diffraction, UV–vis and Raman identified the formation of WO_3 crystallites in all samples prepared by the different methods; however XRD detects a lower formation of WO_3 crystallites in the refluxed samples (Fig. 2). On the other hand, UV–vis shows that the intensity of the absorption edge is higher for samples prepared by impregnation indicating that these samples have higher domain sizes of the WO_x species as two-dimensional polytungstates and three-dimensional WO_3 crystallites. The presence of the polytungstates are not identified by X-ray diffraction, since these WO_x species do not present long range order, but their connectivity could be studied by Raman spectroscopy, since this spectroscopy is able to detect the WO_x with W=O bonds. The W=O bond is related to the formation of tetrahedral and distorted octahedral coordinated tungsten oxide species [4,13,19]. The intensity of the 990 cm^{-1} band is higher in the samples prepared by coprecipitation (Fig. 3) than the impregnated samples, which suggests a high concentration of polytungstates species related to the acid sites [4].

Then, these results show that tungsten is segregated in WO_3 crystallites and disperse in polytungstate species with W=O bonds on the zirconia surface, which has been associated with the formation of the active sites in acidic catalysis, since the supported nanocrystalline structures often exhibit properties different from those observed in microcrystalline structures. Some works have studied the relation between the nanostructures formed on the supported oxides and their catalytic behavior [4,14] and have shown that the reduction of the polymeric species formed on the surface oxides produces the formation of the active sites. Particularly, Barton et al. [4] showed that the structure and catalytic activity of WO_x species on ZrO_2 is controlled only by WO_x surface density (W/nm^2), at intermediate domain sizes these WO_x nanostructures delocalize electron density that is necessary to stabilize the negative charge to form Brönsted acid sites. For the isomerization reactions the maximum reaction rates are reached with densities slightly higher than the polytungstates monolayer [15], however, in the range tested in this work (9–12 W/nm^2), the catalysts with densities near to 12 W/nm^2 presented the best activity in terms of the conversion, reaction rate (as k_w) and selectivity. This behavior is associated with an optimum formation of the polymeric species on the zirconia surface. By using the coprecipitation method, the higher contact of tungstate ions with the $Zr(OH)_4$ increases the amount of condensed polymeric WO_x and three-dimensional WO_x clusters, which are accessible to the reactants and they are reduced, increasing the activity of solids on the *n*-hexane isomerization. The selectivity to isomers is high for all the materials but the coprecipitation method generates higher density of acid sites in the catalysts surface, as it was observed by the rise in the selectivity to biramified products.

The previous analysis shows that Pt/Mn-WO_x-ZrO_2 materials synthesized by coprecipitation using a surfactant assisted synthesis are a good option to be applied in the isomerization of alkanes and a suitable alternative for applications where a specific size of WO_x supported nanostructures is required.

With regard to the catalytic activity of the Pt/Mn-WO_x-ZrO_2 catalysts prepared by different methods, it was found that the catalysts prepared by impregnation showed the lowest *n*-hexane conversion (at 260 °C). Comparing the catalytic activity (at 260 °C) of the catalysts prepared by coprecipitation, the Pt-ZW-COP catalyst showed the lowest conversion (≈43%) and when 0.5% wt of Mn is incorporated, Pt-ZWMn-COP, its activity increases to ≈59%, and modifying the synthesis method in order to enhance the cation interaction, the maximum catalytic activity is reached (≈71%). This behavior can be attributed to the higher formation of strong acid sites on the ZWMn materials, because of both the interaction between the catalytic components by reflux process before to the precipitation of the hydrous zirconia and the Mn incorporation which seem to play the roll of catalytic promoter. On the other hand, the role of the surfactant seems also to be important on catalytic activity and selectivity towards 2,3-DMB and 2,2-DMB because it was found a correlation between the pore size distribution and pore volume (PV) (Fig. 1B) with catalytic activity; the lowest catalytic activity corresponds to the broader PSD and lower PV (ZMWMn-IMP-R), by contrast the highest conversion corresponds to the ZWMn-COP-R, which shows the narrower PSD and highest PV. This result suggests that the mesoporous structure contributes to enhance the catalytic activity of these solids, since it allows better diffusion of the chemical species on the surface of the zirconia improving the dispersion of the WO_x nanocrystalline structures, facilitating the contact with the

dissociated hydrogen provided by the platinum nanocrystals. The selectivity to the 2,3-DMB and 2,2-DMB is higher for the catalysts synthesized by coprecipitation, Mn and reflux. The 2,2-DMB the most kinetically limited increased as higher conversions were reached, according with most accepted mechanism [10,20]. It is worthy to notice that the coprecipitation catalysts were active at 220° and selective to the high octane number 2,3-DMB and 2,2-DMB isomers. The results show that Pt/Mn-WO_x-ZrO_2 materials synthesized by coprecipitation using a surfactant assisted synthesis are a good option to be applied in the isomerization of alkanes and a suitable alternative for applications where a specific size of WO_x supported nanostructures is required.

5. Conclusions

Pt/Mn-WO_x-ZrO_2 solids were found to be efficient catalysts for the *n*-hexane hydroisomerization reaction. However, their catalytic activity is highly dependent to the synthesis method. The results show that the coprecipitation-refluxing method leads to more active and selective catalysts than the materials synthesized by impregnation. Particularly, the ZWMn-COP-R is a good lead for the *n*-hexane hydroisomerization, its catalytic activity and selectivity are high even at 220 °C. The higher activity showed by the catalysts synthesized by coprecipitation may be related to the higher generation of strong acid sites on the catalysts surface, as it was observed by the rise in the selectivity to biramified 2,3-DMB and 2,2-DMB isomers. The mesoporous structure and the narrow pore size distribution of these solids favors the dispersion of the tungsten species and the formation of acid polytungstates species which are accessible and enhances the *n*-hexane hydroisomerization reaction.

The ZrO_2 crystallite morphology at nanometer scale is highly heterogeneous provoking a high dispersion of tungsten oxide and simultaneously favoring a high interaction between the WO_x species and the ZrO_2, this process is enhanced by the coprecipitation refluxing method; it was evidenced by the XRD diffraction, Raman spectroscopy, HRTEM–EDS analysis and the Rietveld refinement. The tungsten polytungstate species favor the catalytic activity. The addition of Mn to the catalysts favor the stabilization of the zirconia in the tetragonal crystalline phase as well as the catalytic activity of these materials.

Acknowledgements

This work was developed with the financial support of the IMP through the projects I.00279 and I.00354 of Combinatorial Chemistry. M.L.H. would also like to acknowledge to CONACYT (no. 128108) and IPN (COFAA and COTEPABE) for the grants received. The authors gratefully acknowledge the technical assistance of the Engineer Ricardo López from the UAM-A in the development of the Raman experiments. We thank Electron Microscopy facilities of Molecular Characterization Laboratory I.00350 at the IMP.

References

[1] J.C. Vartuli, J.G. Santiesteban, P. Traverso, N. Cardona-Martínez, C.D. Chang, S.A. Stevenson, J. Catal. 187 (1999) 131.
[2] J.G. Santiesteban, J.C. Vartuli, S. Han, D. Bastian, C.D. Chang, J. Catal. 168 (1997) 431.
[3] D.G. Barton, S.L. Soled, E. Iglesia, Top. Catal. 6 (1998) 87.
[4] D.G. Barton, M. Shtein, R.D. Wilson, S.L. Soled, E. Iglesia, J. Phys. Chem. B 103 (1999) 630.
[5] M. Hino, K. Arata, J. Chem. Soc. Chem. Commun. (1987) 1259.
[6] S.R. Vaudagna, S.A. Canavese, R.A. Comelli, N.S. Fígoli, Appl. Catal. 168 (1998) 93.
[7] M. Valigi, D. Gazzoli, I. Pettiti, G. Mattei, S. Colonna, S. De Rossi, G. Ferrais, Appl. Catal. A 231 (2002) 159.
[8] C.D. Baertsch, S.L. Soled, E. Iglesia, J. Phys. Chem. B 105 (2001) 1320.
[9] M.L. Hernández, J.A. Montoya, I. Hernández, M. Viniegra, M.E. Llanos, V. Garibay, P. Del Angel, Microporous Mesoporous Mater. 89 (2006) 186.
[10] J.G. Santiesteban, D.C. Calabro, C.D. Chang, J.C. Vartuli, T.J. Fiebig, R.D. Bastian, J. Catal. 202 (2001) 25.
[11] S. Wong, T. Li, S. Cheng, J. Lee, C. Mou, J. Catal. 215 (2003) 45.
[12] X.R. Chen, C.L. Chen, N.P. Xua, S. Han, C.Y. Moub, Catal. Lett. 85 (2003) 177.
[13] S. Kuba, P. Heydorn, R. Grasselli, B.C. Gates, M. Che, H. Knözinger, Phys. Chem. Chem. Phys. 3 (2001) 146.
[14] S. Kuba, P. Lukinskas, R.K. Grasselli, B.C. Gates, H. Knözinger, J. Catal. 216 (2003) 353.
[15] A. Barrera, J.A. Montoya, M. Viniegra, J. Navarrete, G. Espinosa, A. Vargas, P. del Angel, G. Pérez, Appl. Catal. 290 (2005) 97.
[16] N. Naito, N. Katada, M. Niwa, J. Phys. Chem. 103 (1999) 7206.
[17] M. Scheithauer, R.E. Jentoft, B.C. Gates, H. Knözinger, J. Catal. 191 (2000) 271.
[18] J. Liu, Microsc. Microanal. 10 (2004) 55.
[19] M. Scheithauer, R.K. Grasselli, H. Knözinger, Langmuir 14 (1998) 3019.
[20] H.Y. Chu, M.P. Rosynek, J.H. Lunsford, J. Catal. 178 (1998) 352–362.